Nuclear Physics A393 (1983) 237–251

LOW-ENERGY ANTIPROTON ANNIHILATION IN NUCLEI

M. CAHAY, J. CUGNON and J. VANDERMEULEN

Institut de Physique B5, Université de Liège, Sart Tilman, B-4000 Liège 1, Belgique

Received 3 August 1982

Abstract: The annihilation of 100 MeV antiprotons in atomic nuclei is studied in the frame of an intranuclear cascade model. It is found that the antiproton is annihilated about 1 fm inside the nucleus on the average. The energy released by the annihilation is carried by an average of 5 pions, which cascade throughout the nucleus. About 5% (10%) of the primordial pions are absorbed by the ^{40}Ca (^{108}Ag) target. The pions transfer around ~550 MeV (~700 MeV) to the nucleons and eject about one-fifth of the nucleons. The pion and proton cross sections are calculated. In particular, the relative transparency of the nucleus to high-energy pions (and not to pions in the Δ-resonance region) gives rise to a peculiar pion emission pattern. The time evolution of the baryon density and of the spectrum of the participant nucleons is investigated. It turns out that the cascade does not generate high energy density.

1. Introduction

The opening of the LEAR facility in the near future has revived the interest in the interaction of low-energy antiprotons in the nuclei. Several works have been devoted to the estimate of total and annihilation cross sections [1,2]) or to the detail of elastic scattering [3]). The deposit of 2 GeV inside a nucleus opens up interesting prospects, as first underlined by Rafelski [4]), who suggested that antiproton annihilation could excite the nucleus to high temperature or induce a nuclear explosion with a possible shock wave; it could possibly also create large bags from the coalescence of nucleons.

In a previous work [5]), we have investigated the problem by considering antiproton annihilation – emitting 5 energetic pions on the average – at the centre of ^{40}Ca and ^{108}Ag nuclei and studying the outcome by means of an intranuclear cascade (INC) model. Although these central events are not expected to be frequent (with a ~1% probability however in the ^{40}Ca case), they offer the advantage of the optimal geometrical conditions in the prospect of a nuclear explosion. We have found that a density wave travels towards the surface sweeping out about one-fifth of the nucleons. In the process, the pions emitted in the annihilation transfer a substantial amount of their energy to the nucleons.

In the present paper we report on the results of similar calculations, but with the assumption that the impinging antiproton, instead of tunneling to the centre, is free to annihilate in the nucleus according to the $N\bar{N}$ cross section. More precisely, we try to answer the following questions: where does the annihilation take place?

What is the amount of energy transferred from the primordial pions to the nucleon system? What is the final pion multiplicity? We also compute the spectra and angular distribution of pions and protons. But besides the determination of quantities in the final state we also investigate the *time evolution* of the system: of its density, of the pion population, of the number of struck nucleons and of their "temperature" .... This is particularly useful if we try to find out whether the conditions for the creation of large quark bags are realized within nuclei in the course of the interaction process.

These questions, except for the time evolution, are currently studied by the Los Alamos group [6]) and by the Moscow group [7]) (at zero energy), by means of other cascade codes. We will discuss later the differences from our approach. The annihilation process has also been studied by Strottman [8]) in a hydrodynamical model; in particular, he concludes that a sound wave rather than a shock wave propagates inside the nucleus.

Our paper is organized as follows. In sect. 2 we briefly describe the ingredients of our model. Sect. 3 contains our numerical results for 100 MeV $\bar{p}$ annihilation on ^{12}C, ^{40}Ca and ^{108}Ag targets. We successively discuss the properties of the annihilation, the energy transferred to the nucleons, the pion and proton cross sections and the time evolution of the system. Finally, sect. 4 contains our discussion and conclusion.

2. The intranuclear cascade model

Our study of antiproton annihilation inside nuclei is based on the INC model used in ref. [9]), which we have adapted to the present case. The model was constructed to study relativistic nucleus–nucleus collisions, where it is very successful, at least in the GeV range [10]). The nuclei are spherical aggregates of nucleons with uniform density and Fermi motion. The description of the numerical code can be found in refs. [5,9,11]). We give here just a few details concerning the handling of the annihilation and of the pion interaction.

The whole interaction process starts when the antiproton penetrates the nucleus and it is viewed as a succession of *binary* on-shell relativistic baryon–baryon collisions. More precisely, the following reactions are included:

$$\bar{N}N \to \bar{N}N\,, \quad \bar{N}N \to n\pi\,, \quad NN \to NN\,, \quad NN \rightleftarrows N\Delta\,,$$
$$N\Delta \to N\Delta\,, \quad \Delta\Delta \to \Delta\Delta\,, \quad \Delta \rightleftarrows \pi N\,, \quad \pi N \to \pi N\,, \quad \pi N \to \pi\pi N\,. \quad (2.1)$$

For the $\bar{p}$ interaction, we have used isospin-averaged cross sections obtained from ref. [12]). Since we do not distinguish between the charges, the charge-exchange $\bar{p}p \to \bar{n}n$ experimental cross section has been assimilated to elastic scattering. The angular distribution of the $\bar{N}N \to \bar{N}N$ process has been chosen in the form

$$\frac{d\sigma}{d\Omega} \propto e^{A(s)t}\,, \quad (2.2)$$

where t is the four-momentum transfer squared, and $A(s)$ is a function of the c.m. energy which we fitted from data in refs. [12,13]). The pion multiplicity at the annihilation is chosen at random according to a gaussian law in agreement with a fit to at-rest and low momentum $N\bar{N}$ annihilations by a statistical model [14]). The mean value $\langle n \rangle$ and the deviation σ_n have a slight energy dependence. For 100 MeV antiprotons (on a nucleon at rest), $\langle n \rangle = 5.08$ and $\sigma_n = 1.07$. The pion momenta are generated according to constant phase-space density [15,16]), a reasonable approximation for the real situation [17]).

The pion interactions included in the numerical code are described in refs. [5,9]). It is sufficient to say here that the reaction $\pi N \to \Delta$ is effective only in the resonance band $1132\ \text{MeV} < \sqrt{s} < 1300\ \text{MeV}$. Above the latter limit only the reactions $\pi N \to \pi N$ and $\pi N \to \pi\pi N$ are possible. For elastic scattering, we take an angular distribution e^{at}, with $a = 5(\text{GeV}/c)^{-2}$; this value results from an average over the energy interval of interest. The inelastic process is assumed to produce final states according to constant phase space density. The cross sections are taken from ref. [18]) and averaged over isospin states.

We do not consider any potential for any kind of particles, which avoids the problems associated with off-energy-shell collisions. We will come back to this point later on.

The fate of *all* particles is followed during the cascade process both in r-space and in momentum space until the rate of binary interactions becomes negligible. The procedure is repeated a number of times until sufficient statistics is obtained. Typically we have produced 400 runs for each of the 5 input parameters considered in the $\bar{p} + {}^{40}Ca$ case.

3. Numerical results

3.1. ANTIPROTON PENETRATION

The $\bar{N}N$ cross sections are such that the antiproton annihilates at the first interaction about half of the time only. In the other cases, the antiproton scatters elastically once or several times before annihilating; however the antiprotons loose very little energy ($E_{\text{loss}} \simeq 2$–3 MeV) due to the large forward peaking of elastic scattering. We summarize in table 1 the (average) history of 100 MeV antiprotons falling on ^{40}Ca and ^{108}Ag nuclei. In the average, the $\bar{p}$ penetrates $\Delta z \simeq 1$ fm deep inside the nucleus (let us recall that we use sharp-edged densities). The penetration of the incoming $\bar{p}$ is detailed in fig. 1, which gives the distribution of the longitudinal position of the annihilation site for the $\bar{p} + {}^{40}Ca$ case. It does not follow an exponential law at the beginning, i.e. close to the surface. This is a curvature effect: the exponential law would hold for a semi-infinite (i.e. delimited by a plane) medium with constant density; here the antiproton "sees" the matter contained in a cylinder aligned on the incident direction and whose cross section is equal to the $\bar{N}N$ cross section. The

TABLE 1

Average quantities for the 100 MeV antiprotons

^{40}Ca			^{108}Ag		
b (fm)	$\bar{E}_{loss}$ (MeV)	$\overline{\Delta z}$ (fm)	b (fm)	$\bar{E}_{loss}$ (MeV)	$\overline{\Delta z}$ (fm)
0	2.0	0.89	0	2.0	0.87
0.85	2.4	0.88	1.2	1.9	0.74
1.70	2.9	0.90	2.4	2.3	0.91
2.55	2.7	0.97	3.6	2.2	0.90
3.40	2.6	1.07	4.8	2.4	1.01

radius of this cylinder, about 1.7 fm, is not negligible compared to the nuclear radius ($R = 3.83$ fm for ^{40}Ca). Hence, right at the beginning, even an antiproton with $b = 0$ experiences a lesser amount of matter because of the curvature of the nucleus, leading to a maximum in the density of annihilation sites inside the nucleus. One can see, on the other hand, that about 1.5% of the antiprotons come to annihilate within a distance shorter than 1 fm from the ^{40}Ca centre, which brings to ~0.5 mb the total cross section for such central events. This cross section reaches ~3 mb for ^{12}C and practically vanishes for ^{108}Ag.

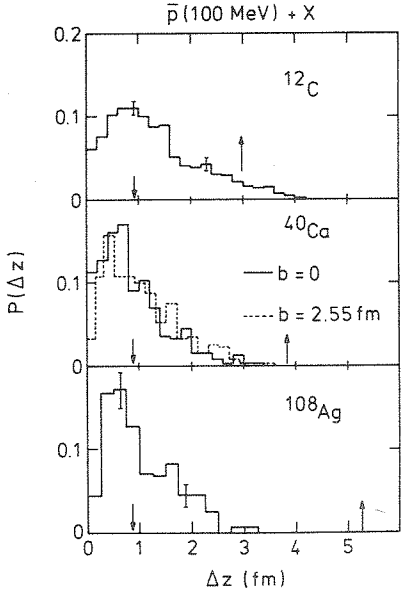

Fig. 1. Location of 100 MeV antiprotons at annihilation by ^{12}C, ^{40}Ca and ^{108}Ag, respectively. The quantity $P(\Delta z)$ is the distribution of Δz, the longitudinal component of the path the antiproton has travelled inside the nucleus. The normalization of $P(\Delta z)$ is such that the sum of the bin heights is equal to one. The downward-pointing arrows give the average value of Δz, whereas the upward-pointing ones indicate the centre of the nucleus (for $b = 0$). The error bars give typical uncertainties of the calculation.

3.2. THE TRANSFORMATION OF THE PRIMORDIAL PIONS

The annihilation of 100 MeV antiprotons releases 2 GeV in the form of pions (5 on the average) emitted isotropically in the $\bar{p}$-nucleon frame. In the annihilation of an antiproton at rest at the edge of the nucleus, ~2.5 pions are emitted outwards and would not interact at all. In our actual case, this escape effect is reduced for two reasons: (i) the annihilation frame moves with respect to the lab (or nucleus) frame with a velocity $\beta \simeq 0.22$ and (ii) the annihilation takes place, as we have seen, *inside* the nucleus. In our picture, the pions interact with the nucleons mainly through Δ-formation and subsequent decay, since many primordial pions have their energy in the Δ-region, where the cross section is quite large. To fix the ideas, the annihilation on a ^{40}Ca nucleus at zero impact parameter is followed by 7.8 Δ-formations and 6.9 Δ-decays, on the average. The other reactions controlling the Δ-population occur with the following frequencies: 0.31 for $\pi N \rightarrow \pi\pi N$, 0.68 for $N\Delta \rightarrow NN$ and 0.04 for $NN \rightarrow N\Delta$. In addition, high energy pions make, on the average, 1.9 elastic scatterings on the nucleons. The evolution of the π and Δ-populations as well as the rate of the various reactions are grossly similar to what is found for central annihilations [5]). In particular, the maximum number of Δ's present at a time in the system is around 1.5 and occurs about 3 fm/c after the annihilation.

In table 2 we show the final pion multiplicities (for all charge states) and the energy (in the lab frame) carried out by these pions. About 5% of the primordial pions disappear in the ^{40}Ca nucleus. This fraction reaches ~10% in ^{108}Ag, a direct consequence of the size of the system. Likewise, the energy contained in the final pion system W_{tot} is larger for ^{40}Ca than for ^{108}Ag; in other words, the energy transferred from the pion system (i.e. from the $N\bar{N}$ annihilation) to the nucleons E_{tr} is larger for heavier nuclei. E_{tr} is defined as the difference between the total lab energy of the $N\bar{N}$ pair and W_{tot}, the sum of the energies of the pions (including

TABLE 2

Final average pion multiplicity and average total pion energy for 100 MeV antiproton annihilation

^{40}Ca			^{108}Ag		
b (fm)	$\langle M_\pi \rangle$	$\langle W_{tot} \rangle$ (MeV)	b (fm)	$\langle M_\pi \rangle$	$\langle W_{tot} \rangle$ (MeV)
0	4.71	1381	0	4.43	1210
0.85	4.75	1414	1.2	4.43	1204
1.70	4.80	1427	2.4	4.47	1276
2.55	4.70	1445	3.6	4.54	1312
3.40	4.67	1545	4.8	4.56	1390
average over b	4.73	1457	average over b	4.51	1303

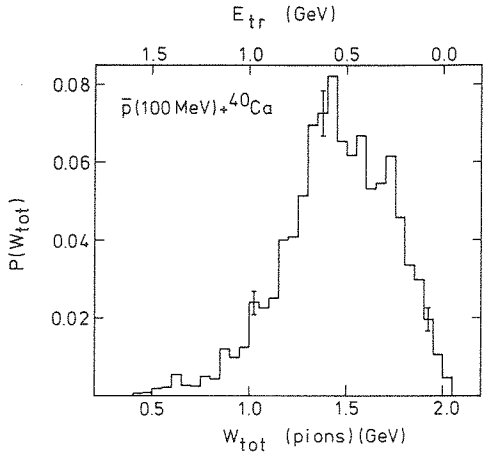

Fig. 2. Distribution of the total energy W_{tot} carried by the final pions after the annihilation of 100 MeV $\bar{p}$ on ^{40}Ca nuclei. The normalization of $P(W_{tot})$ is such that the sum of the bin heights is equal to one.

mass) in the same frame. It amounts to ~550 MeV in ^{40}Ca, on the average, and to ~700 MeV in ^{108}Ag. However, the transferred energy fluctuates very much as shown in fig. 2 for annihilation on ^{40}Ca (all impact parameters considered); the pion system may transfer as much as 1.6 GeV to the nucleon system. Fig. 3 gives

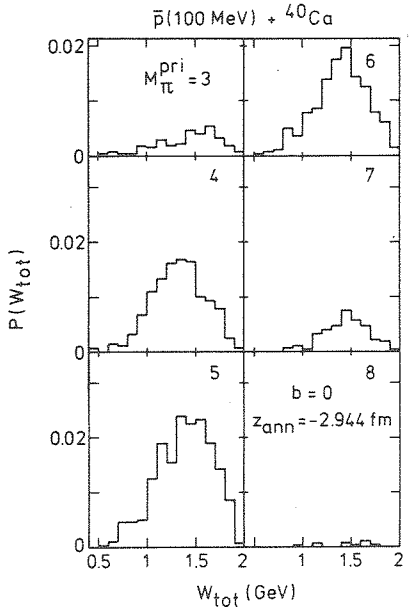

Fig. 3. Same as fig. 2, but the events have been split according to the value of the primordial pion multiplicity.

finer detail of the pion energy distribution: the latter is split according to the multiplicity of the primordial pions. The energy loss does not depend very much upon the initial multiplicity M_π^{pri}, except for $M_\pi^{\mathrm{pri}} = 3$: in this case, the pions are quite energetic, well above the resonance, and are thus less likely to interact.

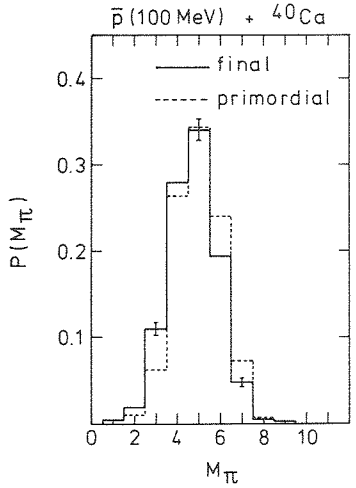

Fig. 4. p̄ (100 MeV) annihilation on ^{40}Ca nucleus: primordial and final pion multiplicity distribution. Error bars give typical uncertainities of the calculation.

We compare the final pion multiplicity M_π (all charge states) with the primordial one in fig. 4. The high multiplicities are depleted in favour of the low (3, 4) ones. This results mainly from an overall absorption, blended with a small multiplicity-dependent effect. When the primordial multiplicity increases, the average initial pion energy decreases and more pions have their energy in the resonance region, resulting in a larger absorption. For $n = 3$ on the other hand the pions are well above the resonance and fly through a rather transparent nucleus; as a consequence the $M_\pi = 2$ yield is not increased very much. Furthermore, the $\pi N \to \pi\pi N$ reaction is mainly effective for low M_π^{pri} events, and thus helps to limit the $M = 2$ yield.

A matter of great interest is how the energy transferred to the nucleons is dissipated. In our simple picture of incoherent binary collisions, the energy is carried by the nucleons which are involved in at least one collision (i.e. the participant nucleons in the language of relativistic heavy ion physics). To avoid ambiguities arising from the absence of a potential well in our model, we adopt here a stronger definition for the participants, namely: those nucleons having acquired a momentum larger than 300 MeV/c. We see from table 3 that the number of participants is about one-fifth of the total number of nucleons, as in central annihilations [5]). There is a slight decrease for peripheral collisions, since the pions have then more chance to escape before interacting.

TABLE 3

Average number of participant nucleons N_p

^{12}C	b (fm)	0	0.65	1.3	1.95	2.6
	N_p	3.67	3.694	3.598	3.448	3.106
^{40}Ca	b (fm)	0	0.85	1.70	2.55	3.4
	N_p	9.47	9.13	9.20	8.89	8.25

3.3. THE CROSS SECTIONS

We start with the pion spectrum in the lab frame, i.e. the double differential cross section $d^2\sigma/dE\, d\Omega$ integrated over all directions; as before, all charge states are included. Fig. 5 shows the energy distribution divided by a kinematical factor which would entail an exponential law, should the pion system reach thermal equilibrium. This is clearly not the case, for two reasons. The incident energy of 100 MeV, although in the lower band of energies planned at LEAR, imparts an overall flow in the forward direction. The second reason accounts for the presence of the high energy ($\geqslant$250 MeV) tail of the spectrum: this stems from the high energy primordial pions which, with a total cross section of the order of 40 mb, travel through a relatively transparent nuclear matter.

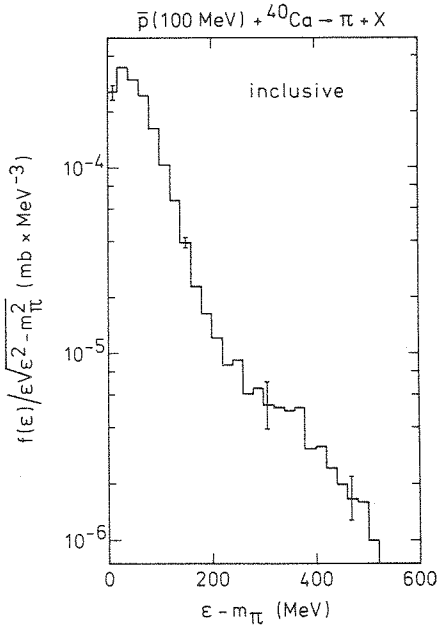

Fig. 5. Pion spectrum $f(\varepsilon)$ after 100 MeV $\bar{p}$ annihilation on ^{40}Ca. The quantity $f(\varepsilon)$ is normalized to the total pion (all charge states) cross section.

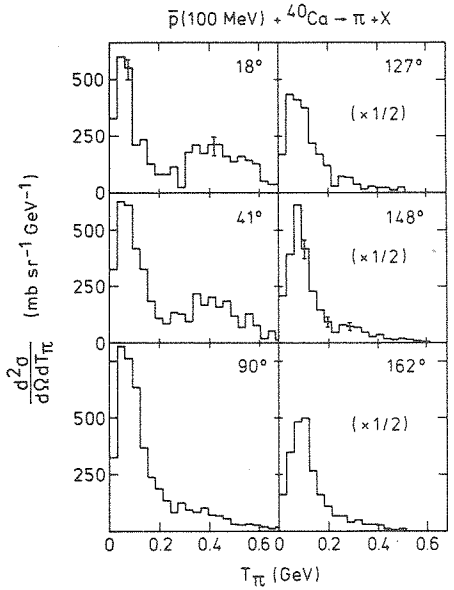

Fig. 6. Double differential lab cross section for pion (all charge states) production following the $\bar{p}$ annihilation on ^{40}Ca nuclei. The quantity T_π is the pion kinetic energy. The error bars give the typical uncertainties of the calculation.

Fig. 6 provides more insight on the interactions of the pions; it shows the pion spectrum at different angles. Surprisingly enough, the high energy tail is more important at forward angles. This contradicts the simple-minded picture of an antiproton annihilating at the surface and producing free (thus faster) pions in the backward hemisphere. Our result is nevertheless understandable on the basis of two observations: (i) the annihilation occurs *inside* the nucleus; (ii) pion emission is isotropic in a frame moving with a non-negligible velocity with respect to the lab frame. For 100 MeV antiprotons, β is around 0.22. Let us then consider pions with a typical total energy of 400 MeV in the N$\bar{\text{N}}$ frame: for a pion emitted forwards, the lab energy is 507 MeV; on the other hand a backward-emitted pion has 333 MeV only. This entails an important effect: the forward pions are well beyond the resonance while the backward ones fall just in the resonance region; as they have to cross ~0.9 fm of nuclear matter they easily loose energy.

Fig. 6 also reveals that the pions *which have been slowed down* are more numerous in the backward hemisphere. This effect of preferential backward reemission is clearly exhibited by fig. 7, which shows the pion angular distribution (for zero impact parameter). To prevent the dispersion of annihilation sites to possibly dilute some features of the phenomenon, we have – for the sake of this figure – repeated the calculation forcing the antiproton to annihilate at 2.944 fm from the nucleus centre, i.e. at the average annihilation site (see fig. 1). The dashed curve shows the

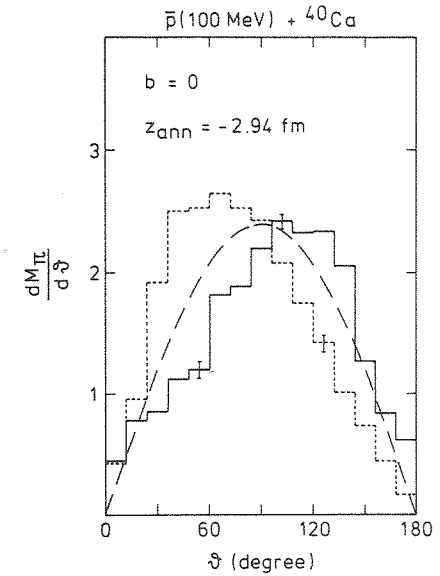

Fig. 7. Primordial (dotted line) and final (full line) angular distributions for pion production following $\bar{p}$ (100 MeV) annihilation on ^{40}Ca nuclei. The antiproton is assumed to collide with zero impact parameter and annihilate at 2.944 fm from the centre of the nucleus. See text. The dashed line corresponds to an isotropic emission in the lab system.

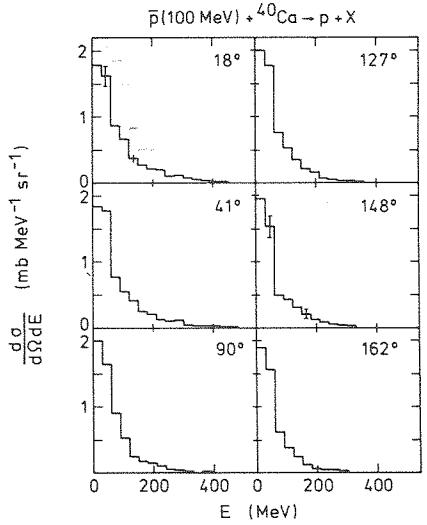

Fig. 8. Double differential cross section for proton emission following the $\bar{p}$ (100 MeV) annihilation in ^{40}Ca nuclei.

angular distribution (in the lab frame) of the primordial pions; the full curve is for the final pions. There is an overall reduction of ~5% (see table 2) due to pion absorption. But there appears a clear depletion of the forward yield in favour of the backward hemisphere. We will see later on that the evolution of the density could play an important role in this effect.

The proton double differential cross section is displayed in fig. 8 for several angles. Proton emission is roughly isotropic; the only interesting feature is the fact that $d^2\sigma/dE\, d\Omega$ as a function of E falls down faster at backward angles. The spectra can be fitted more or less by Maxwell–Bolzmann distributions, the associated temperatures (as extracted from the high energy tail) varying from $T \simeq 65$ MeV (± 5 MeV) in the forward direction down to $T \simeq 43$ MeV (± 5 MeV) in the backward one. We believe it is a direct consequence of the motion of the annihilation frame: in the lab frame there is more energy available forwards than backwards. For the sake of comparison, the temperature which can be tentatively associated to the low-energy part of the pion spectrum (fig. 5) is 55 MeV $\pm$ 8 MeV. The temperatures that we give here should be considered as a measure of the dispersion in energy and do not necessarily imply that the pions or the protons have reached thermal equilibrium.

3.4. THE TIME EVOLUTION OF THE SYSTEM

According to ref. [4]), an attractive feature of antiproton annihilation by nuclei is the possibility of studying the nuclear equation of state in conditions different from those encountered in relativistic nuclear collisions. The matter is expected to be heated without too much compression. The hydrodynamical calculation of ref. [8]) suggests however an already large compression, the density reaching a maximum of about $1.8\,\rho_0$, ρ_0 being the normal nuclear matter density. The results of the INC calculation are rather different, as already underlined in our study of central annihilation [5]). In fig. 9 we give the curves of constant baryon density at different times during the annihilation process of a 100 MeV antiprotons in ^{40}Ca. Once again, to focus on the studied effect, we show the results of a calculation where the $\bar{p}$, coming from the top, is found to annihilate at the fixed distance of 2.94 fm ahead of the centre. The pions create in the nucleus a kind of crater which develops forwards but is however progressively filled up. The maximum density is around $1.15\,\rho_0$, which is remarkably small, and it occurs for $t \simeq 2$ fm/c. The compression is much smaller than in an hydrodynamical picture, because the cascade calculation concentrates energy in point-like pions which may exchange energy with the surrounding matter without disturbing many nucleons at the same time.

The depletion in the back of the nucleus, which is fully developed after a few fm/c, may enhance the emission of final pions from Δ-decays in the backward direction, as we have suggested in subsect. 3.3.

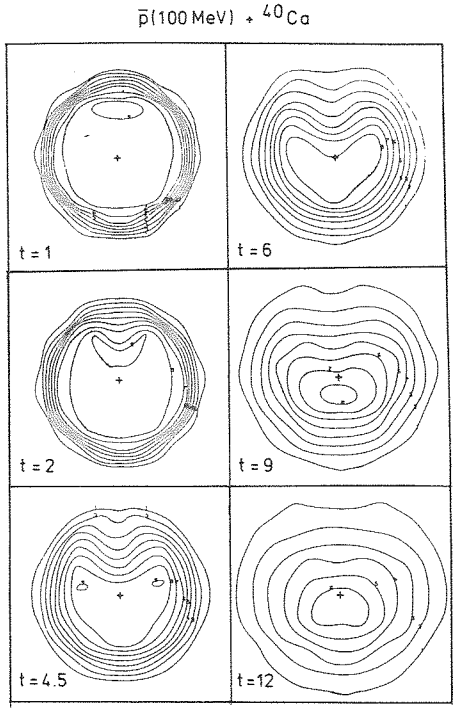

Fig. 9. Contour plot of the baryon density at different moments during the interaction process. The 100 MeV antiproton is assumed to come from the top of the figure with a zero impact parameter and annihilate at $t = 0$ and at a 2.94 fm distance from the centre of the nucleus (indicated by the crosses). The density increases when going inwards. The lines correspond to densities of $1, 2, 3, \ldots$ times $0.02\ \mathrm{fm}^{-3}$, successively. The side of each square is 11.6 fm long.

In fig. 10, we display the time evolution of the system of participants. The number of struck nucleons N_p (including Δ's) increases steadily; this results from the combined effect of pion interactions and of NN elastic collisions, which help to share the energy received from the pions amongst more nucleons. The upper part of the figure gives an idea of the time variation of the energy gained by the participants. In fact, the tail of the transverse momentum spectrum can be satisfactorily fitted by a function associated to the Maxwell–Boltzmann distribution. The quantity T_0 is the extracted "temperature" and is rather time-independent. This observation and fig. 9 together show that, in the cascade following the annihilation, there is no situation with high energy density. It seems that within this model the conditions are not realized for a transition to a quark–gluon plasma [19]). They however are sufficient to allow the transition to quark–gluon blobs as described by Rafelski [20]).

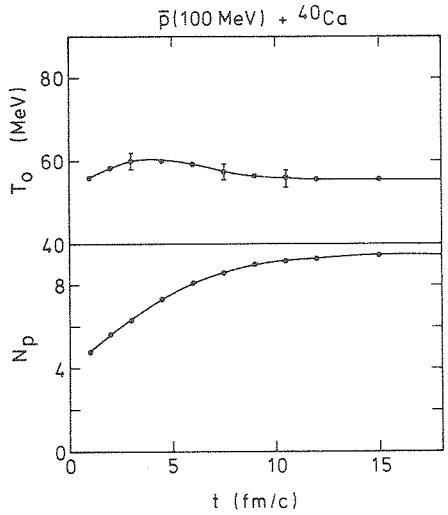

Fig. 10. Time evolution of the number of participant nucleons (lower part) and of their "temperature" as extracted from the transverse momentum spectra (see text). The parameters of the collision are the same as in fig. 9.

4. Discussion

We have investigated here a cascade model for the antiproton annihilation. The basic assumption of the model is the possibility of describing the process as a succession of binary relativistic on-shell collisions which proceed as in free space. This assumption is of limited value for the initial stage of the process, namely the propagation of the antiproton inside the nucleus and its annihilation. The reason is the large total $\bar{N}N$ cross section, which makes very probable a (possibly coherent) interaction of the antiproton with several nucleons at the same time. A similar uncertainty affects the annihilation process whose main properties (pion multiplicity, pion spectrum, . . .) could be changed by the surrounding matter. In particular, the energy released by the annihilation may very well be distributed from the very beginning on a cluster containing pions (possibly in a nascent form) and surrounding nucleons, rather than on ~5 point-like well defined particles. Even more, the accurate description of the system during a time interval short after the annihilation may require the introduction of the quark degrees of freedom. Therefore, our calculation should be seen as a zeroth order picture, based on conventional and simple concepts. It can be considered as a description of the "background" on which exotic processes would hopefully leave a neat signature.

For the description of the cascade following the annihilation, the INC model is on safer grounds; although the condition of large mean path which has to be required is marginally fulfilled. Yet the comparison with the calculation of ref. [6]), which is based on the same ideas, reveals that the INC model is not as unique as

one may think at first. Let us discuss a little bit the differences between the two calculations. Contrary to ref. [6]), we do not introduce an attractive potential for the antiproton. The latter could be very deep [1,2,3]). If true, this is rather embarrassing for a cascade approach, because one has to consider off-the-mass shell collisions, for which the cross sections may be different from those observed on the mass-shell ones. But we think that this can just affect the total cross section. Indeed, an attractive potential bends the $\bar{p}$ trajectory inwards and the latter appears as corresponding to a smaller effective impact parameter. As we have seen, the gross features (number of participants, pion multiplicity, etc. . . .) do not depend very much upon the impact parameter.

We similarly neglect the potential well for protons and pions. Hence, the low-energy part of the spectra for these particles (especially for the protons) should not be taken too seriously. Also we do not include evaporation processes, which, on the scale of fig. 8, would only affect the first bin of the histograms.

The calculation of ref. [6]) and ours include essentially the same interactions, except for the πN interactions above the Δ-resonance region. We have not enough information to decide whether the associated cross sections are exactly the same in both calculations. However, they are not expected to differ very much. The results are in gross agreement (the backward escape of the slow pions is clearly present in both calculations), except for a definite difference in the number of participants. Although we consider different targets, it is clear that their figure is smaller than ours. Correlatively, the average proton temperature in ref. [6]) (between $\sim$82 MeV for ^{12}C to $\sim$70 MeV for ^{238}U) is significantly larger than the temperature we have indicated ($T \sim 55$ MeV for ^{40}Ca). We have no clear explanation for this discrepancy. It could come from a different handling of the interaction between cascading particles as well as from a different description of the interaction of high energy pions with the nucleons. There is little overlap between ref. [7]) and our work, since the former deals with $\bar{p}$ annihilation at rest at the surface of the nucleus. As we have seen there is a definite effect brought in by the velocity of the antiproton with respect to the target.

In conclusion, we have studied a possible scenario for the antiproton annihilation, which can be summarized as (i) a straight line motion of the incoming particle in the nucleus with a path given by the free-space annihilation cross section, followed by (ii) an annihilation on a single nucleon which distributes the $\bar{N}$N total energy among an average of 5 point-like pions, and (iii) cascades of these pions inside the target, in the form of a sequence of hadron–hadron collisions. The third stage of the scenario seems to us the most reliable. An alternative picture is offered by the hydrodynamical approach of ref. [8]). The two approaches make different predictions, the most important of which is, according to us, the number of participants. Due to a large transparency effect, only about one-fifth of the nucleons are disturbed in our scenario whereas the whole nucleus is involved in an hydrodynamical model. Note, however, the prediction of the number of participants is also the most obvious

difference between the results of ref. [6]) and ours. Unfortunately, the number of participants is probably the observable which will be the most affected by the occurrence of an annihilation mechanism different from the one assumed in our scenario (as we hope it is the case). If the annihilation involves several nucleons at the same time, the number of participants will probably change, since the initial perturbation will already be different. Also, if the annihilation gives rise to a shaking of the pion (and possibly other boson) field, extending on a large region of space, instead of materializing immediately in 5 pions, the number of participants and the number of pions in this case will be changed. All these considerations call for measurements of pion and proton multiplicities and for refinements of the theoretical calculations.

References

1) N.J. di Giacomo, J. Phys. **G7** (1981) L169
2) A. Bouyssy and S. Marcos, Orsay preprint IPNO/TH82-10 (1982), Phy. Lett. 114B (1982) 349
3) E.H. Auerbach, C.B. Dover and S.H. Kahanna, Phys. Rev. Lett. **46** (1981) 702
4) J. Rafelski, Phys. Lett. **91B** (1980) 281
5) M. Cahay, J. Cugnon, P. Jasselette and J. Vandermeulen, Phys. Lett. **115B** (1982) 7
6) M.R. Clover, R.M. DeVries, N.J. Di Giacomo and Y. Yariv, preprint LA-UR-82-1398 (1982)
7) A.S. Iljinov, V.I. Nazaruk and S.E. Chigrinov, Nucl. Phys. **A382** (1982) 378
8) D. Strottman, Los Alamos preprint (1981)
9) J. Cugnon, D. Kinet and J. Vandermeulen, Nucl. Phys. **A379** (1982) 553
10) J. Cugnon, Phys. Rev. **C22** (1980) 1885
11) J. Cugnon, T. Mizutani and J. Vandermeulen, Nucl. Phys. **A352** (1981) 505
12) Particle Data Group, $\bar{N}N$ and $\bar{N}D$ Interactions. A compilation, LBL-58 (1972)
13) CERN-HERA 79-03, Compilation of cross-sections. p and $\bar{p}$ induced reactions (1979)
14) J. Vandermeulen, Nuovo Cim. Lett. **11** (1974) 243; **28** (1980) 60
15) E. Fermi, Progr. Theor. Phys. **5** (1950) 570
16) P.P. Srivastava and G. Sudarshan, Phys. Rev. **110** (1958) 765
17) C. Ghesquière, Symposium on antinucleon–nucleon interactions, Cern Yellow Report 74-18, p. 436
18) CERN-HERA 79-01, Compilation of cross-sections I. π^- and π^+ induced reactions (1979)
19) J. Engels, F. Karsch and H. Satz, Phys. Lett. **113B** (1982) 398
20) J. Rafelski, preprint UFTP 73-1982.